International Journal of Microwave and Wireless Technologies

cambridge.org/mrf

Ultra-compact self-diplexing antenna based on quarter-mode substrate integrated waveguide with high isolation

Ayman A. Althuwayb

Department of Electrical Engineering, College of Engineering, Jouf University, Sakaka, Aljouf 72388, Kingdom of Saudi Arabia

Research Paper

Cite this article: Althuwayb AA (2022). Ultra-compact self-diplexing antenna based on quarter-mode substrate integrated waveguide with high isolation. *International Journal of Microwave and Wireless Technologies* **14**, 926–931. https://doi.org/10.1017/S1759078721001173

Received: 7 March 2021
Revised: 4 July 2021
Accepted: 15 July 2021
First published online: 12 August 2021

Keywords:
antenna; quarter-mode substrate integrated waveguide; self-diplexing

Author for correspondence:
Ayman A. Althuwayb,
E-mail: aaalthuwayb@ju.edu.sa

Abstract

This article presents the design of an ultra-compact cavity-backed self-diplexing antenna with high isolation employing quarter-mode substrate integrated waveguide (QMSIW). The proposed antenna is constructed by using QMSIW, slot, and two 50Ω feed lines. Two eighth-mode cavity resonators are designed by inserting a slot on the top side of the rectangular substrate integrated waveguide to operate at 2.6 and 4.9 GHz for long-term evolution and public safety band applications, respectively. The proposed design allows to tune any frequency band independently by keeping other bands unaltered. The size of antenna is ultra-compact, due to the use of QMSIW cavity. The isolation between two ports is >35 dB. The antenna achieves 5.34 and 5.68 dBi peak gains at 2.6 and 4.9 GHz, respectively. The efficiency of the antenna is >85% at both frequency bands. The antenna provides more than 20.9 dB front-to-back-ratio and better than 21 dB separation between co-to-cross polarization levels. The designed antenna is validated through fabrication and measurement.

Introduction

The recent development in modern communication systems demands compact, low-loss, and multi-frequency antennas for multi-standard applications. On the other hand, multiple transceivers require high isolation when combined for RF front-end systems. The substrate integrated waveguide (SIW) is a promising technology for the development of low-loss, compact circuit size, and high-performance antennas [1, 2]. In the literature, several antennas are designed by employing SIW technology [3–9]. In [3], a quadrant sector of cavity resonator called quarter-mode SIW (QMSIW) has been exploited for the development of circular polarized antenna. In [4], a dual-band array antenna has been realized using SIW with longitudinal slots for Ku-band applications. In [5], a dual-band antenna array has been designed by applying QMSIW for 5G applications. In [6], an antenna based on SIW with single-slot has been implemented for dual-frequency applications. In [7], a SIW antenna for dual-frequency and flexible polarization has been realized based on composite right/left-handed topology. In [8], a dual-frequency antenna has been implemented by using SIW with triangular-slot. In [9], a dual-frequency antenna has been designed based on the SIW with four conductive-slots and two orthogonal feed lines for flexible polarization. These antennas exhibit excellent performances. For multi-standard applications, multiple transceivers containing these antennas were unable to provide sufficient isolation. Additional frequency-selective devices (multiplexer circuits) are employed to enhance the isolation which increases the circuit size and complexity. Therefore, self-diplexing antennas based on SIW dispense compact size, low-loss, and does not require additional frequency-selective devices.

In recent years, many self-diplexing antennas have been realized based on SIW technology [10–15]. In [10], a self-diplexing antenna has been designed based on SIW with a bowtie-shaped slot. In [11], two transverse-slots placed on the top of the SIW cavity with two feed lines have been employed for the development of self-diplexing antenna. In [12], a self-diplexing antenna has been realized by using a plus-shaped slot on the SIW cavity. In [13], a rectangular-slot has been etched on the top of SIW cavity to design a self-diplexing antenna. In [14], a self-diplexing antenna has been realized based on SIW with U-shaped slot for compact size and high isolation. In [15], a self-diplexing antenna has been designed based on SIW cavity with bowtie-ring slot and orthogonal feed lines. These SIW cavity-backed antennas exhibit excellent performance indicators (such as circuit size, isolation, gain, front-to-back-ratio (FTBR), co-to-cross polarization and radiation characteristics) but limit the application due to larger electrical size and low isolation. Therefore, novel techniques need to be exploited for the development of ultra-compact and high-performance self-diplexing SIW antennas.

© The Author(s), 2021. Published by Cambridge University Press in association with the European Microwave Association

CAMBRIDGE UNIVERSITY PRESS

In this article, a novel design of ultra-compact self-diplexing antenna with high isolation employing QMSIW is presented. The antenna is excited by two independent 50Ω orthogonal feed lines. Two eighth-mode cavity resonators (EMCRs) are formed on the top of the QMSIW for radiating at 2.6 and 4.9 GHz. These frequency bands can be tuned independently. The proposed antenna is validated through fabrication and measurement. The features of the antenna are highlighted as follows:

(1) Compared to the existing self-diplexing antennas reported in [8–15], the size of the proposed antenna is ultra-compact due to the use of QMSIW.
(2) The antenna achieves high isolation (>35 dB) between two ports when compared with the previously reported works [8–15].
(3) The antenna achieves good peak gains, FTBRs, and co-to-cross polarization levels when compared to existing works [8, 9].
(4) The antenna exhibits more than 85% efficiency with such a highly miniaturized antenna.
(5) Keeping one frequency band unaltered, other frequency bands can be designed independently.
(6) The performances of the designed antenna are validated through fabrication and measurement.

Configuration and analysis of the proposed antenna

The configuration of the proposed self-diplexing cavity-backed antenna is illustrated in Fig. 1. The antenna is constructed using QMSIW, a slot, and two 50Ω independent feed lines. The slot is engraved on the top side of the QMSIW to form two EMCRs. These EMCRs are excited by two independent 50Ω feed lines for radiating at two distinct frequencies. The antenna is realized to operate at 2.6 and 4.9 GHz for long-term evolution (LTE) and public safety band (PSB) applications, respectively. This antenna is realized on 0.787 mm thick 5870 RT/Duriod substrate with ϵ_r = 2.33 and tanδ = 0.002.

Initially, a full-mode SIW (FMSIW) cavity ($W_{eff}^{FMSIW} \times L_{eff}^{FMSIW}$) is designed to operate TE_{110} mode at 3.4 GHz following the design equations in [14]. This FMSIW is divided into two equal parts, each part is called as half-mode SIW (HMSIW). Then the HMSIW is divided into two halves to produce QMSIW. The resonant frequencies of each SIW cavity is determined by following [3]:

$$f_{mn0}^{FMSIW} = \frac{1}{2\pi\sqrt{\varepsilon_r}}\sqrt{\left(\frac{m\pi}{W_{eff}^{FMSIW}}\right)^2+\left(\frac{n\pi}{L_{eff}^{FMSIW}}\right)^2} \quad (1)$$

$$W_{eff}^{FMSIW} = W_{SIW} - 1.08\frac{d^2}{p} + 0.1\frac{d^2}{W_{SIW}} \quad (2)$$

$$L_{eff}^{FMSIW} = L_{SIW} - 1.08\frac{d^2}{p} + 0.1\frac{d^2}{L_{SIW}} \quad (3)$$

$$W_{eff}^{HMSIW} = \frac{W_{eff}^{FMSIW}}{2} + \Delta W_{add} \quad (4)$$

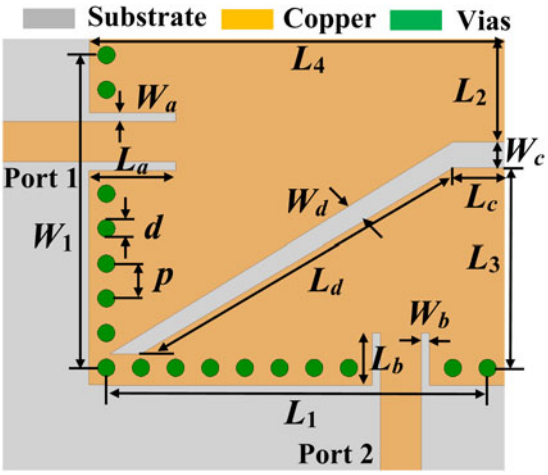


Fig. 1. Schematic of QMSIW cavity-backed slot antenna. Final dimensions: L_1 = 22, W_1 = 18, L_2 = 6.0, L_3 = 12.5, L_4 = 24, L_a = 5.0, W_a = 0.5, L_b = 3.0, W_b = 0.5, L_c = 3.0, W_c = 1.5, L_d = 20.95, W_d = 1.8, d = 1.0, p = 2.0 (units: millimeters).

$$\Delta W_{add} = hs\left(0.05+\frac{0.3}{\varepsilon_r}\right)\times \ln\left(0.79\frac{W_{eff}^{FMSIW}}{4hs}+\frac{52W_{eff}^{FMSIW}-261}{hs^2}+\frac{38}{hs}+2.77\right) \quad (5)$$

$$f_{mn0}^{QMSIW} = \frac{1}{2\pi\sqrt{\varepsilon_r}}\sqrt{\left(\frac{m\pi}{W_{eff}^{QMSIW}}\right)^2+\left(\frac{n\pi}{L_{eff}^{QMSIW}}\right)^2} \quad (6)$$

$$W_{eff}^{QMSIW} = W_{eff}^{HMSIW} \quad (7)$$

$$L_{eff}^{QMSIW} = L_{eff}^{HMSIW} \quad (8)$$

The proposed antenna is designed using a QMSIW as illustrated in Fig. 2. Figure 3 shows the electric field distributions for SIW, HMSIW, and QMSIW resonators at 3.4, 6, and 3.35 GHz, corresponding to the TE_{110}^{FMSIW}, TE_{110}^{HMSIW}, and TE_{110}^{QMSIW}, respectively. The resonating frequencies of HMSIW and QMSIW resonators slightly differ with respect to FMSIW due to the fringing field at the open edges. The electric field distribution of the QMSIW without slot in TE_{110} mode at 3.35 GHz and the frequency response are depicted in Fig. 4. Next, a slot is introduced on the top side of the QMSIW cavity to obtain two EMCRs for radiating at two different frequency bands. The resonating frequencies of top-side and bottom-side EMCRs can be determined by:

$$f_{mn0}^{TopEMCR} = \frac{1}{2\pi\sqrt{\varepsilon_r}}\sqrt{\left(\frac{m\pi}{2W_1}\right)^2+\left(\frac{n\pi}{2L_4}\right)^2} \quad (9)$$

$$f_{mn0}^{BottomEMCR} = \frac{1}{2\pi\sqrt{\varepsilon_r}}\sqrt{\left(\frac{m\pi}{2L_1}\right)^2+\left(\frac{n\pi}{2L_3}\right)^2} \quad (10)$$

Where m = n = 1, 2,…, and ϵ_r be the relative permittivity of the substrate. The size of the EMCRs are made different to achieve

https://doi.org/10.1017/S1759078721001173 Published online by Cambridge University Press

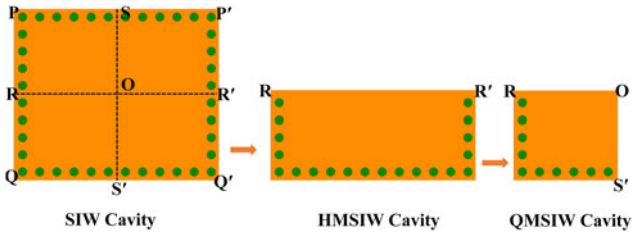


Fig. 2. Conversion of SIW to QMSIW cavity.

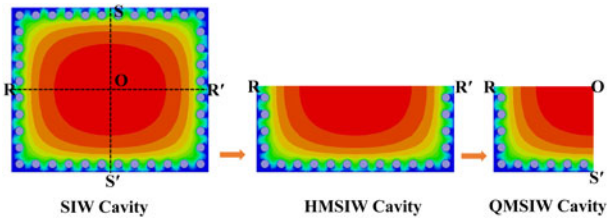


Fig. 3. E-field distribution of SIW, HMSIW, and QMSIW cavities.

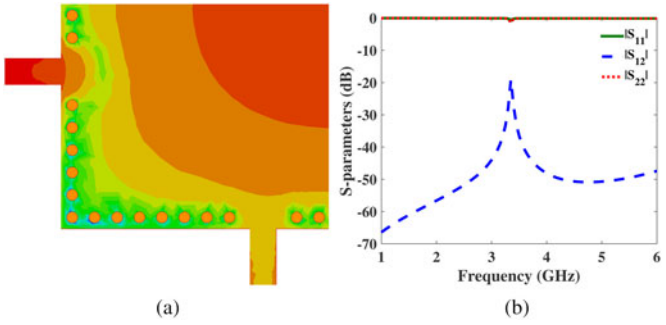


Fig. 4. (a) E-field distribution of the QMSIW without slot in TE_{110} mode at 3.35 GHz and (b) its frequency response.

distinct frequency bands. The top-side and bottom-side EMCRs are responsible for radiation at 2.6 and 4.9 GHz. These frequency bands can be designed independently by varying the dimensions of the EMCRs. The full-wave performances of the proposed antenna are depicted in Fig. 5. The antenna achieves better than −20 dB return loss and more than 34 dB port isolation. High isolation is achieved due to the weak cross-coupling path between two 50Ω orthogonal feed lines. The electric and magnetic field distributions are illustrated in Figs 6 and 7, respectively. It is seen that the maximum E-fields are observed at the outer-edge of the top side and bottom side of the EMCRs.

The variation of radiating bands due to the parameters L_2, L_3, and L_4 are studied. To reconstruct the radiating bands (f_1 and f_2), the parameters L_2, L_3, and L_4 can be varied individually/simultaneously as per the application requirements. Due to the variation of dimension of the parameters L_2, L_3, and L_4, the capacitive loading on the cavity is modified which results in tuning of radiating frequencies. The tuning of first radiating band is determined by varying the parameters L_2 and L_4 as shown in Fig. 8. It is observed that the first radiating band is shifted toward left when the parameters L_2 and L_4 increase without altering the second radiating band. The first radiating band can be tuned in the frequency range of 2.56–2.78 when L_2 (L_4) varied from 6.0 to 4.0 mm (23.9 to 21.5 mm). Similarly, the designing of second radiating

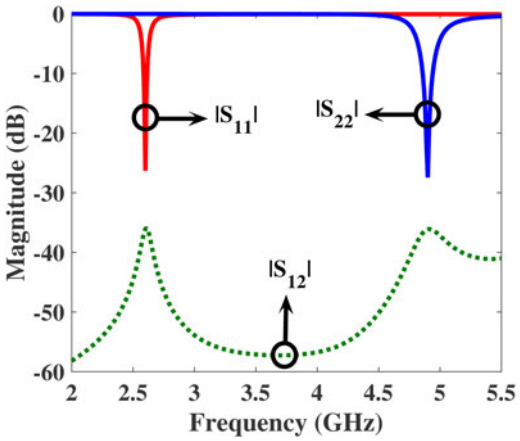


Fig. 5. Simulation responses of the proposed QMSIW antenna.

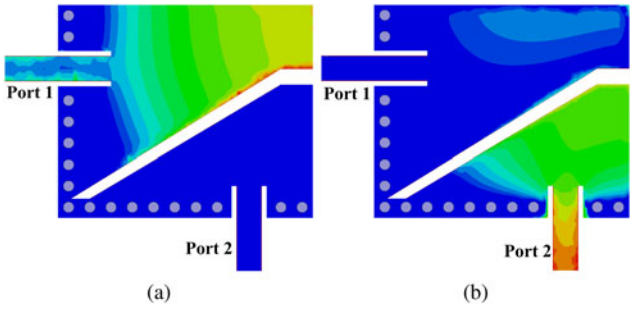


Fig. 6. Electric-field distributions. (a) At 2.6 GHz. (b) At 4.9 GHz.

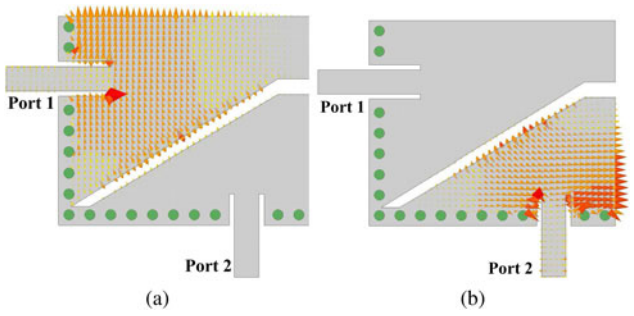


Fig. 7. Magnetic-field distributions. (a) At 2.6 GHz. (b) At 4.9 GHz.

band is realized by varying the parameter L_3 as depicted in Fig. 9. From the figure, it is seen that the second radiating band is shifted toward right when the parameter L_3 decreases without any effect on the first radiating band. The second operating band can be tuned in the frequency range of 4.87–5.13 when the parameter L_3 varied from 12.3 to 10.7 mm. Therefore, the radiating frequency bands can be designed independently/simultaneously by varying the dimensions of the EMCRs as per applications.

Based on the above studies, a simple design approach has been suggested.

(1) Select the dimension of the FMSIW cavity by following the design equations for resonant frequency (1)–(3).
(2) Produce HMSIW by symmetrical cutting of the FMSIW. This HMSIW is then cut symmetrically to form QMSIW.

https://doi.org/10.1017/S1759078721001173 Published online by Cambridge University Press

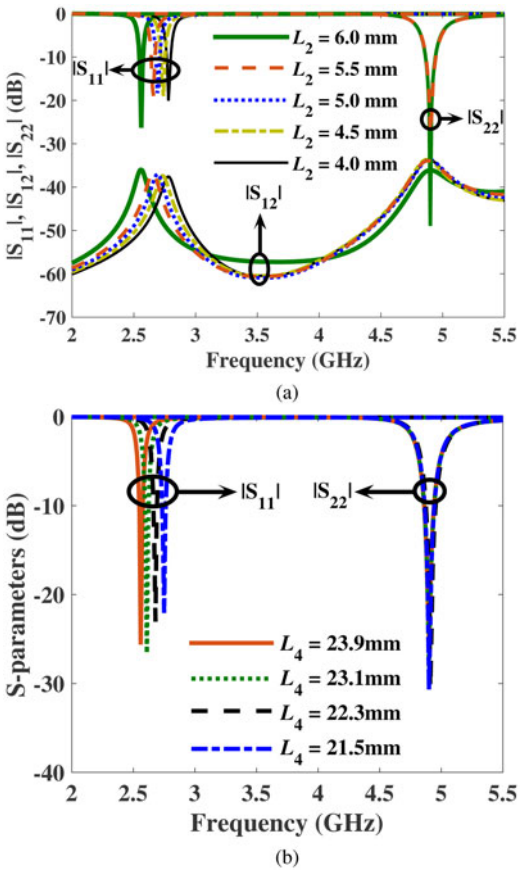


Fig. 8. Tuning of first resonating frequency. (a) Due to L_2. (b) Due to L_4.

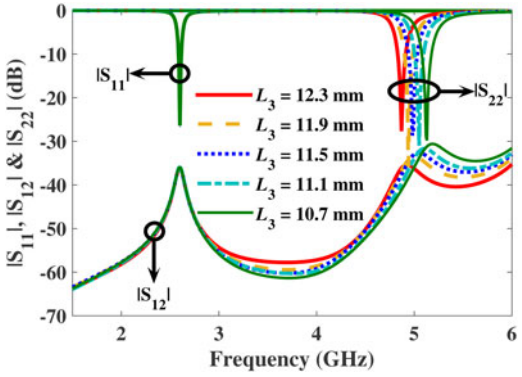


Fig. 9. Tuning of second resonating frequency.

(3) The resonant frequencies of the HMSIW and QMSIW are determined by using the equations (4)–(8).
(4) Insert a slot on the top surface of the QMSIW to construct two EMCRs which exhibit the self-diplexing characteristic.
(5) Select the dimension of the top EMCR responsible for first radiating band as $0.22\lambda_g \times 0.29\lambda_g$.
(6) Select the dimension of the top EMCR responsible for second radiating band as $0.28\lambda_g \times 0.50\lambda_g$.
(7) Optimize the parameters L_a and L_b to achieve proper impedance matching.
(8) Vary the parameters L_2, L_3, and L_4 for designing of radiating frequency bands independently.

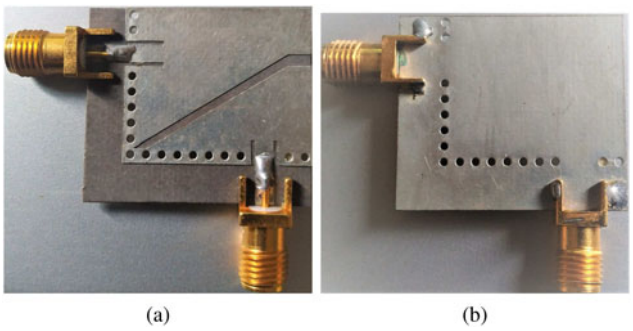


Fig. 10. Fabricated prototype. (a) Front view. (b) Back view.

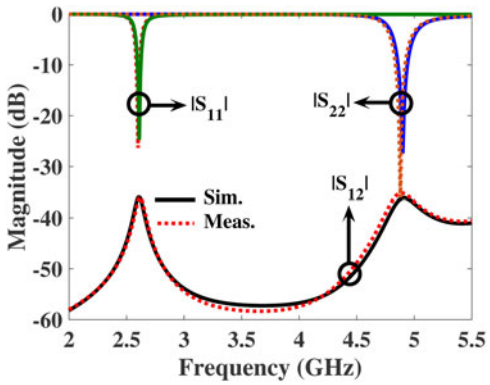


Fig. 11. Full-wave simulated and measured magnitude responses of the suggested SDA.

(9) Repeat last two steps to obtain the desired antenna characteristics.

Fabrication, measurement, and comparative analysis

To support the theoretical analysis, the proposed antenna is fabricated and demonstrated for LTE and PSB applications. Figure 10 shows the photograph of the fabricated antenna. All the experiments are carried out by employing excitation at one port and terminating the other port by 50Ω load. The input matching and isolation are measured using Rohde and Schwarz vector network analyzer. Figure 11 depicts the performances of the full-wave simulated and measured reflection coefficients ($|S_{11}|$ and $|S_{22}|$) and isolation ($|S_{12}|$). The far-field performances of the fabricated prototype in two-orthogonal planes of $\Phi = 0^\circ$ and $\Phi = 90^\circ$ at 2.6 and 4.9 GHz are demonstrated inside an anechoic chamber. The full-wave simulated and measured peak gains and radiation efficiency are illustrated in Figs 12 and 13, respectively. The full-wave simulated and measured radiation patterns of the fabricated antenna at 2.6 and 4.9 GHz are depicted in Figs 14 and 15, respectively. The measured and full-wave simulated performances are very consistent as expected. However, very small deviation is seen between full-wave simulated and measured performances due to fabrication tolerance and connector loss. The performances of the fabricated prototype are summarized as follows:

(1) Simulation
  (a) The input return losses $|S_{11}|$ and $|S_{22}|$ are better −22 dB.
  (b) The port isolations are 36.07 and 36.13 dB at 2.6 and 4.9 GHz, respectively.

https://doi.org/10.1017/S1759078721001173 Published online by Cambridge University Press

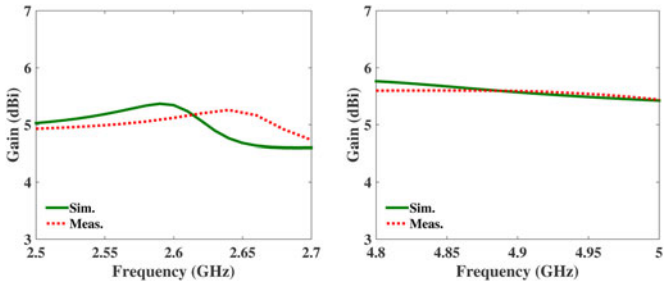


Fig. 12. Full-wave simulated and measured gain.

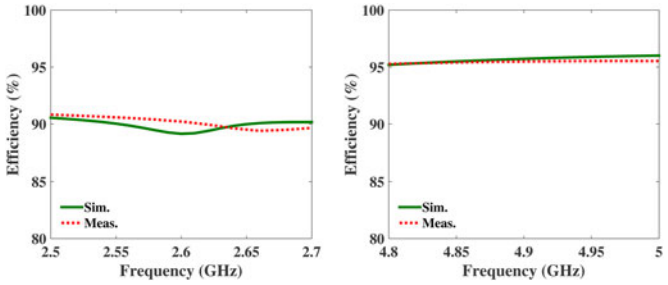


Fig. 13. Full-wave simulated and measured efficiency.

(c) The full-wave peak gains are 5.34 and 5.56 dBi at 2.6 and 4.9 GHz, respectively.
(d) The radiation efficiencies of the proposed antenna are 89.1and 95.7% at 2.6 and 4.9 GHz, respectively.
(e) The FTBR and co-to-cross polarization level are better than 22 and 20 dB, respectively.

(2) Measurement
(a) The return losses $|S_{11}|$ and $|S_{22}|$ of the fabricated antenna are > -21 dB at all the radiating frequencies.
(b) The port isolations ($|S_{12}|$) of the fabricated antenna are found to be 36.69 and 35.23 dB at 2.6 and 4.9 GHz, respectively.
(c) The measured peak gains are 5.12 and 5.59 dBi at 2.6 and 4.9 GHz, respectively.
(d) The measured radiation efficiencies of the fabricated antenna are 90.2 and 95.4% at 2.6 and 4.9 GHz, respectively.
(e) The FTBR and co-to-cross polarization level are very consistent to the full-wave simulated performances.

A comparative analysis is discussed on performance indicators (size, isolation, peak gain, return loss and FTBR) between the proposed antenna and previously reported works. Table 1 illustrates the performance comparison of state-of-the-art dual-frequency antennas. Compared to [8–15], the proposed prototype is ultra-compact. The size of the manufactured antenna is 74.3% smaller than the most compact self-diplexing antenna reported in [14].

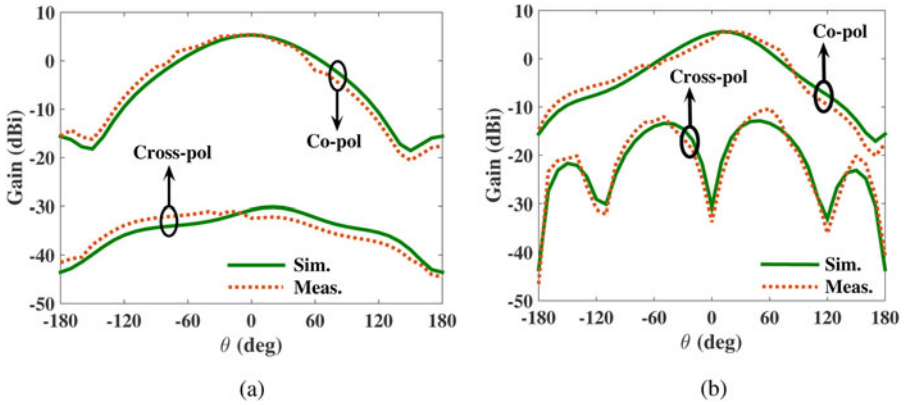


Fig. 14. Full-wave simulated and measured radiation pattern at 2.6 GHz. (a) E-plane ($\phi = 0^{\circ}$). (b) H-plane ($\phi = 90^{\circ}$).

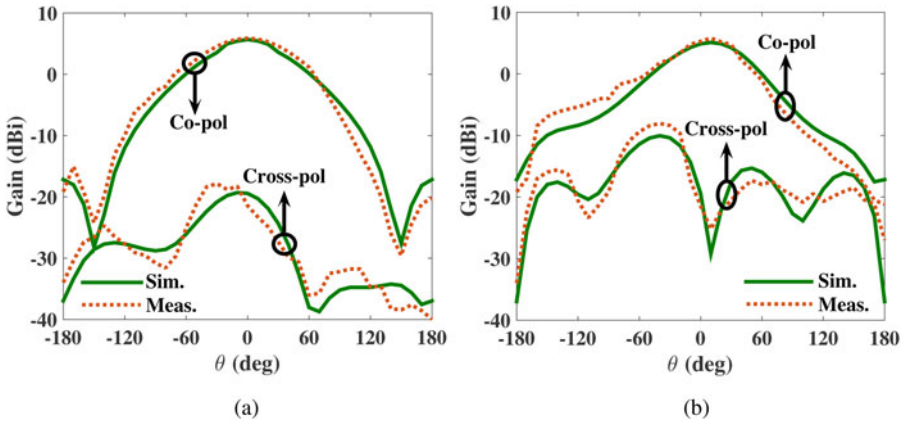


Fig. 15. Full-wave simulated and measured radiation pattern at 4.9 GHz. (a) H-plane ($\phi = 0^{\circ}$). (b) E-plane ($\phi = 90^{\circ}$).

https://doi.org/10.1017/S1759078721001173 Published online by Cambridge University Press

Table 1. Performance comparison between proposed and previously reported self-diplexing antennas

Ref.	Techn.	Freq. (GHz)	Thickness (mm)	ϵ_r	Isolation (dB)	Gain (dBi)	FTBR (dB)	Size (λ_g^2)
[8]	SIW	9.4/16.2	1.57	2.2	>13	4.86, 6.15	18, 18	0.621
[9]	SIW	13.4/17.9	1.575	2.2	>20	NM	NM	1.053
[10]	SIW	9/11.2	0.787	2.2	>25	4.3, 4.2	21, 16	0.95
[11]	SIW	8.26/10.46	1.57	2.2	>27.9	3.56, 5.24	23, 20	0.43
[12]	SIW	8.55/9.77	1.57	2.2	>18	5.7, 5.94	12, 23	0.607
[13]	SIW	9.5/10.5	1.58	2.2	>29	5.55, 5.75	NM	0.796
[14]	SIW	4.29/7.52	0.787	2.33	>32.8	5.38, 5.82	23, 22	0.23
[15]	SIW	6.62/11.18	0.787	2.33	>29.3	5.42, 5.66	23, 21	0.362
This work	QMSIW	2.6/4.9	0.787	2.33	>35.2	5.34, 5.68	20.9, 22	0.059

The proposed antenna achieves highest port isolation when compared with [8–15]. The antenna exhibits good peak gain, FTBR, and co-to-cross polarization level when compared with existing works in [8–15]. Therefore, the proposed self-diplexing cavity-backed QMSIW slot antenna is suitable for dual-frequency compact communication systems.

Conclusions

In this article, the design of a ultra-compact high-isolation cavity-backed self-diplexing antenna employing QMSIW for LTE and PSB applications is presented. The proposed antenna is configured by utilizing a QMSIW, one slot, and two 50Ω feed lines. A slot is placed on the top side of the QMSIW to produce two EMCRs for radiating at 2.6 and 4.9 GHz. These frequency bands can be designed individually by varying the dimensions of the eighth-mode resonators. For validation, the suggested antenna is fabricated and demonstrated. The size of the fabricated prototype is ultra-compact due to the utilization of QMSIW cavity. The port isolation is better than 35 dB at all the radiating bands. The fabricated prototype exhibits good peak gain, FTBR, and co-to-cross polarization levels along with efficiency >85% at all the frequency bands.

Acknowledgment. The authors extend their appreciation to the Deanship of Scientific Research at Jouf University for funding this work through research grant No (DSR-2021-02-0212).

References

1. **Bozzi M, Georgiadis A and Wu K** (2011) Review of substrate-integrated waveguide circuits and antennas. *IET Microwaves, Antennas and Propagation* **5**, 909–920.
2. **Xu F and Wu K** (2005) Guided-wave and leakage characteristics of substrate integrated waveguide. *IEEE Transactions on Microwave Theory and Techniques* **53**, 66–73.
3. **Jin C, Li R, Alphones A and Bao X** (2013) Quarter-mode substrate integrated waveguide and its application to antennas design. *IEEE Transactions on Antennas and Propagation* **61**, 2921–2928.
4. **Wei DJ, Li J, Yang G, Liu J and Yang JJ** (2020) Design of compact dual-band SIW slotted array antenna. *IEEE Antennas and Wireless Propagation Letters* **17**, 1085–1089.
5. **Deckmyn T, Cauwe M, Ginste DV, Rogier H and Angeessens S** (2019) Dual-band (28,38) GHz coupled quarter-mode substrate-integrated waveguide antenna array for next-generation wireless systems. *IEEE Transactions on Antennas and Propagation* **67**, 2405–2412.
6. **Jiang W, Huang K and Liu C** (2018) Ka-band dual-frequency single-slot antenna based on substrate integrated waveguide. *IEEE Antennas and Wireless Propagation Letters* **17**, 221–224.
7. **Lee H, Ren D and Choi JH** (2018) Dual-band and polarization flexible CRLH substrate-integrated waveguide resonant antenna. *IEEE Antennas and Wireless Propagation Letters* **17**, 1469–1472.
8. **Zhang T, Hong W, Zhang Y and Wu K** (2014) Design and analysis of SIW cavity backed dual-band antennas with a dual-mode triangular-ring slot. *IEEE Transactions on Antennas and Propagation* **62**, 5007–5016.
9. **Lee H, Sung Y, Wu CM and Itoh T** (2016) Dual-band and polarization flexible cavity antenna based on substrate integrated waveguide. *IEEE Antennas and Wireless Propagation Letters* **15**, 488–491.
10. **Mukherjee S and Biswas A** (2016) Design of self-diplexing substrate integrated waveguide cavity-backed slot antenna. *IEEE Antennas and Wireless Propagation Letters* **15**, 1775–1778.
11. **Nandi S and Mohan A** (2017) An SIW cavity-backed self-diplexing antenna. *IEEE Antennas and Wireless Propagation Letters* **16**, 2708–2711.
12. **Nandi S and Mohan A** (2018) SIW-based cavity-backed self-diplexing antenna with plus-shaped slot. *Microwave and Optical Technology Letters* **60**, 827–834.
13. **Khan AA and Mandal MK** (2019) Compact self-diplexing antenna using dual-mode SIW square cavity. *IEEE Antennas and Wireless Propagation Letters* **18**, 343–347.
14. **Barik RK, Cheng QS, Dash SKK, Pradhan NC and Karthikeyan SS** (2020) Design of a compact orthogonal fed self-diplexing bowtie-ring slot antenna based on substrate integrated waveguide. *International Journal of RF and Microwave Computer-Aided Engineering* **30**, e22422.
15. **Barik RK, Cheng QS, Dash SKK, Pradhan NC and Karthikeyan SS** (2020) Compact high-isolation self-diplexing antenna based on SIW for C-band applications. *Journal of Electromagnetic Waves and Applications* **34**, 960–974.



Ayman A. Althuwayb received the B.Sc. degree (Hons.) in electrical engineering (electronics and communications) from Jouf University, Saudi Arabia, in 2011, the M.Sc. degree in electrical engineering from California State University, Fullerton, CA, USA, in 2015, and the Ph.D. degree in electrical engineering from Southern Methodist University, Dallas, TX, USA, in 2018. He is currently an Assistant Professor with the Department of Electrical Engineering at Jouf University, Kingdom of Saudi Arabia. His current research interests include antenna design and propagation, microwaves and millimeter-waves, wireless power transfer, ultrawideband and multiband antennas, filters, and others.

https://doi.org/10.1017/S1759078721001173 Published online by Cambridge University Press